

Enzymatic cycle-based receivers with high input impedance for approximate maximum a posteriori demodulation of concentration modulated signals

Chun Tung Chou

School of Computer Science and Engineering, University of New South Wales, Sydney, New South Wales
2052, Australia.

E-mail: c.t.chou@unsw.edu.au

Abstract—Molecular communication is a bio-inspired communication paradigm where molecules are used as the information carrier. This paper considers a molecular communication network where the transmitter uses concentration modulated signals for communication. Our focus is to design receivers that can demodulate these signals. We impose three features on our receivers. We want the receivers to use enzymatic cycles as their building blocks, have high input impedance and can work approximately as a maximum a posteriori (MAP) demodulator. No receivers with all these three features exist in the current molecular communication literature. We consider enzymatic cycles because they are a very common class of chemical reactions that are found in living cells. Since a receiver is to be placed in the communication environment, it should ideally have a high input impedance so that it has minimal impact on the environment and on other receivers. Lastly, a MAP receiver has good statistical performance. In this paper, we show how we can use time-scale separation to make an enzymatic cycle to have high input impedance and how the parameters of the enzymatic cycles can be chosen so that the receiver can approximately implement a MAP demodulator. We use simulation to study the performance of this receiver. In particular, we consider an environment with multiple receivers and show that a receiver has little impact on the bit error ratio of a nearby receiver because they have high input impedance.

Keywords: Molecular communications; maximum a posteriori; enzymatic cycles; demodulation; input impedance; molecular computation; analog computation; molecular circuits.

I. INTRODUCTION

Molecular communication is a bio-inspired communication paradigm where the transmitters and receivers use molecules to communicate with each other [1], [2], [3]. One can take this bio-inspiration a step further by considering the fact that living cells encode and decode molecular signals by using molecular circuits, or sets of chemical reactions. This has motivated researchers in molecular communications to study and design chemical reaction-based transmitters and receivers [4], [5], [6]. This paper focuses on designing a reaction-based demodulator for molecular communications.

There is a growing list of work in molecular communications that uses reaction-based receivers. Kuscu and Akan [7] designed a molecular circuit that can extract information from

multiple types of ligand. We designed a molecular circuit which can approximately perform maximum a posteriori (MAP) demodulation [8] and we shown later on in [9] that the circuit can be implemented by gene promoters with multiple binding sites. Bi et al. [10] designed a molecular receiver which uses a catalytic-like reaction to amplify the received molecular signal and the concept was later implemented in a microfluidic testbed in [11]. Heinlein et al. [12] derived a reaction-based realisation of the MAP demodulator by exploiting a connection between MAP and Boltzmann machines. A gap in the existing literature on reaction-based receiver design is that none of the designs is based on enzymatic cycles (e.g. phosphorylation-dephosphorylation cycles, methylation-demethylation cycles) which are a very common class of chemical reactions in the living cells [13]. In addition, synthetic biologists have started to build synthetic protein circuits [14]. A goal of this paper is to study how receivers based on enzymatic cycles can be designed.

This paper is built upon the framework in our earlier work [15], [16] which uses a Markovian approach to design MAP demodulators. The work [16] assumes that the receiver consists of two blocks in series: a front-end and a back-end, as in Fig. 1. The front-end is a molecular circuit which reacts with the signalling molecules from the transmitter to produce output molecules. The back-end works as a MAP demodulator by using the number of output molecules over time to compute the the log-posteriori probabilities of the possible transmission symbols. The contribution of [16] is to derive an ordinary differential equation (ODE) which governs the time-evolution of the log-posteriori probabilities given the front-end molecular circuit. Note that the results in [16] are very general as the front-end can be any set of chemical reactions. Since our goal is to design a receiver that uses enzymatic cycles, we will choose the front-end to be an enzymatic cycle. We will argue in this paper that a desirable property of the front-end is that it has a high input impedance so that it has a minimum impact on the environment that it observes. We will derive the conditions required by an enzymatic cycle to have high input impedance. We then use the results in [16] to derive the ODE for computing the

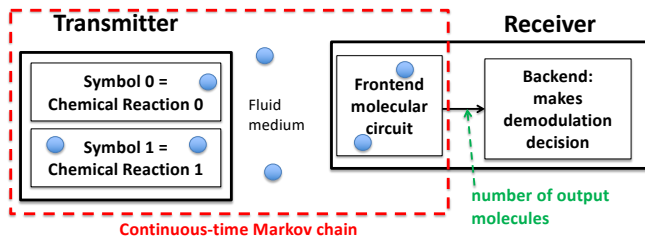


Fig. 1: Overview of the communication elements.

log-posteriori probabilities. We will show how we can use enzymatic cycles to approximately realise this ODE. This paper makes the following contributions:

- We show that we can realise an enzymatic cycle with high input impedance by appropriately choosing the time scales of its reaction rate constants.
- We derive a method to approximately compute the log-posteriori probabilities which will later on lead to an implementation using enzymatic cycles. The approximation consists of multiple steps. In one of these steps, we derive a closed-form approximation of an optimal Bayesian filtering problem. In another step, we show how high input impedance can lead to a simplification of log-posteriori probability computation.
- We design an enzymatic circuit, which is composed of three enzymatic cycles, that can approximately compute the ratio of log-posteriori probabilities. We demonstrate the accuracy of this approximation using simulation.
- We show that the enzymatic circuit can function well in a multi-receiver environment where a receiver has little impact on the bit error ratio (BER) of a nearby receiver.

The rest of the paper is organised as follows. Sec. II discusses related work. In Sec. III, we present the set up of our molecular communications problem and relevant background results from [16]. Sec. IV present results on input impedance, log-posteriori probability approximation and the design of the enzymatic circuit. We then present simulation results in Sec. V and conclude in Sec. VI.

II. RELATED WORK

There are many surveys on molecular communications, some of these surveys discuss extensively on the use of chemical reactions in molecular communications, e.g., [4], [5], [6]. We have already discussed some existing work [7][10][11][12] on designing chemical reaction-based receivers in the introduction. Some other similar work is [17], [18], [19], [20]. This paper differs from these earlier papers in two key aspects. First, the earlier work assumed that the demodulation is based on one sample point per symbol; however, this work assumes that demodulation is based on the continuous history of the number of active receptors. We showed in [8] that demodulation using a continuous history gives a lower BER in comparison. Second, the molecular demodulator considered in earlier work did not use enzymatic

cycles. To the best of our knowledge, there is few work [21] [22] on considering the use of enzymatic cycles in molecular communication; however, the prior work is focused on channel capacity, rather than the design of enzymatic circuits.

In the molecular communication literature, molecular circuits have been studied for various applications. For example, [23], [24] present genetic circuits for parity-check. As another example, [25], [26] studied molecular circuits for inter-cellular communication and targeted drug delivery, however their analysis is based on deterministic models rather than stochastic models which are used in this paper.

Although most of the work that uses chemical reactions in molecular communication is focused on the receiver side, there is also work that consider reaction-based transmitters and medium. For example, [27] uses chemical reactions to produce transmission signals for molecular communication, [28] considers a transmitter that uses ion channels, [29] considers the use of chemical reactions in the channel to improve communication performance. There is few work in molecular communications that studies the interaction between multiple reaction-based receivers. An early work is [30]. A recent work [31] models the interaction between multiple absorbing receivers which can be considered to be a special type of chemical reactions.

Synthetic biologists have found that the connection of a downstream molecular component to an upstream molecular circuit can have an adverse effect on the behaviour of the upstream circuit. The review paper [32] discusses these adverse effects in the context of molecular communications. The paper [22] studies the impact of the inter-connection of enzymatic circuits on mutual information. In this paper, we use time-scale separation to achieve high input impedance to minimise the impact of upstream enzymatic cycles.

III. MODEL AND EXACT COMPUTATION OF POSTERIORI PROBABILITIES

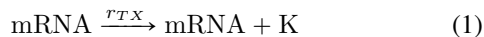
This section presents the set up of the following three components in our molecular communication system: the medium, the transmitter and the front-end of the receiver. Note in particular, the front-end of the receiver is an enzymatic cycle. By using this set up and our earlier work [16], we present an ODE which describes the evolution of posteriori probability over time. This ODE forms the basis of this paper and our goal is to show how we can realise this ODE by using enzymatic cycles in Sec. IV.

A. Transmission Medium and Transmitter

The modelling framework of this paper mostly follows our previous work [15][33]. We model the medium as a rectangular prism and divide the medium into voxels. We assume that the transmitter and the receiver each occupies a voxel. Note that it is possible to generalise to the case where a transmitter or receiver consists of multiple voxels, see [34], but we have not done that to simplify the presentation.

Although it may not be physically realistic for the receiver to have a cubic shape, this simplified geometry allows us to focus on the signal processing aspect of the receiver.

We assume the transmitter communicates with the receiver using one type of signalling molecule K, which is depicted as blue circles in Fig. 1. The transmitter uses $S = 2$ different symbols indexed by $s = 0, 1$. (Generalisation to the $S > 2$ case is left for further research.) We assume that the transmitter uses concentration shift keying where each symbol s is characterised by a constant mean production rate of signalling molecules and each symbol is produced by a chemical reaction, see Fig. 1. An example of a reaction that can produce molecules at a constant mean rate is:



where r_{TX} denotes the reaction rate constant. In this reaction, signalling molecules are produced at a mean rate of r_{TX} times the concentration of the mRNA molecules. Without loss of generality, in this paper, we assume the transmitter uses (1) as the reaction and the transmission symbol $s = 0$ (resp. $s = 1$) is produced by using a lower (higher) mRNA concentration with a common r_{TX} for the two reactions. Note that it is straightforward to generalise the results in this paper to other transmitter reactions as long as they produce the signalling molecule at a mean constant rate. Lastly, we assume that once the signalling molecules have been produced, they are free to diffuse in the medium.

B. Receiver front-end molecular circuit

The receiver front-end is assumed to be an enzymatic cycle which reacts with the signalling molecule K. The cycle consists of three species X, XK and X_* which take part in the following four reactions:



where a_0 , d_0 , g_0 and g_- are reaction rate constants. In the case where the above reactions are of the phosphorylation-dephosphorylation reaction type, then we identify X, K, XK and X_* as, respectively, a unphosphorylated substrate, kinase, complex and phosphorylated substrate [35]. We assume that the *substrate* — which is the collection of all the species that has an X in them, i.e., X, XK and X_* — can only be found in the receiver and cannot be diffused outside of the receiver.

We assume the signalling species K can freely diffuse in and out of the receiver. Since the transmitter emits signalling molecules K at different rates for Bits 0 and 1, this will create different concentration levels of K in the receiver voxel. We would like the reactions in (2) to produce a low (resp. high) number of X_* when Bit 0 (Bit 1) is sent to enable the receiver to infer the bit that the transmitter has sent by using the amount of X_* . In fact, one may consider the front-end as a device to measure the concentration of K.

We want this device to be sensitive to the amount of K but at the same time it should have little effect on the quantity that it measures. These requirements are similar to that of a voltmeter which is required to have both high sensitivity and high input impedance so that it has little influence on the circuit being measured. We will show in Sec. IV-A how we can choose the rate constants in (2) to achieve both high sensitivity and input impedance.

We have now described the transmitter, the medium and the receiver front-end. These system components have reactions (e.g., the production of K in the transmitter voxel and reactions (2) in the receiver voxel) and diffusion of the signalling molecule K. We model the dynamics of these three components (which is the dashed box in Fig. 1) by using the reaction-diffusion master equation (RDME)¹ [38], which is a specific type of continuous-time Markov chain. The receiver back-end is used for MAP demodulation, which will be discussed in Sec. III-D.

C. Notation

We will deal with time-varying chemical signals in this paper. For a chemical species, we will use its species name in *italics* font to denote its count. For example, the count of X_* molecules in the receiver at time t is denoted by $X_*(t)$. This applies to all chemical species with one letter. For chemical species with multiple letters, we add curly brackets $\{ \}$ around their name, e.g. $\{XK\}(t)$ is the molecular count of the species XK at time t .

We will use quasi-steady state analysis [37] to help us to understand the properties of the receiver. Typically quasi-steady analysis expresses its results in concentration. We will denote the concentration of a species by enclosing its name within a pair of square brackets $[]$, e.g. $[X_*]$ denotes the concentration of X_* . For the RDME model, both molecular counts and concentration are studied at the spatial scale of a voxel and we can convert between them using the volume of a voxel Ω , e.g. $[X_*] = \frac{X_*}{\Omega}$.

We add the superscript ^{ss} to a quantity to denote its steady state mean value, e.g. X_*^{ss} is the mean number of X_* molecules at steady state.

Sometimes we may need to express the molecular count of a particular species due to a specific transmission symbol s where $s \in \{0, 1\}$. In that case, we add s , 0 or 1 as a subscript to indicate that, e.g., $X_{*,1}^{\text{ss}}$ is the steady state count of X_* when symbol 1 is transmitted.

The signalling molecule K diffuses in the medium so each voxel has its own molecular count of K. However, the results

¹There are three major classes of stochastic models for modelling systems with both diffusion and reactions. They are the Smoluchowski equation, RDME and the Langevin equation [36]. The Smoluchowski equation is based on particle dynamics. It is a fine grained model but hard to work with analytically. Both RDME and Langevin are easier to work with analytically but master equation has a finer scale and granularity compared to the Langevin equation [37]. Therefore we choose to use RDME which allows us to use Markovian theory for analysis and is at the same time a finer grained model.

will only require us to consider the count or concentration of K in the receiver voxel. We will use $K(t)$, $[K]$ to indicate the count and concentration K in the receiver voxel.

Lastly, the total count of some species may be conserved in the receiver voxel. For example, the total count of X, XK and X_* is a constant. We use X_T and $[X]_T$, with a subscript T which is short for “total”, to denote the conserved total count and concentration.

D. MAP Demodulation: Problem and Solution

In this paper, we consider a demodulation problem of using the information on X_* to infer the symbol that the transmitter has sent. We will focus on the demodulation of one symbol and we assume that there is no inter-symbol interference.

In the formulation of the demodulation problem, we will assume that at time t , the data available to the demodulation problem are $X_*(\tau)$ for all $\tau \in [0, t]$; in other words, the data are continuous in time and are the history of the counts of X_* up to time t . We will use $\mathcal{X}_*(t)$ to denote the continuous-time history of $X_*(t)$ up to time t . Given that we model the molecular communication system using RDME, this means that $X_*(t)$ is a realisation of a continuous-time Markov chain.

We adopt a MAP framework for detection. Let $\mathbf{P}[s|\mathcal{X}_*(t)]$ denote the posteriori probability that symbol s has been sent given the history $\mathcal{X}_*(t)$. Since we assume the transmitter uses only 2 symbols, the demodulation decision can be made from using the log-probability ratio $L(t)$:

$$L(t) = \log \left(\frac{\mathbf{P}[1|\mathcal{X}_*(t)]}{\mathbf{P}[0|\mathcal{X}_*(t)]} \right) \quad (3)$$

If the demodulation decision is to be done at time t , then the demodulator decides that Symbol 1 has been sent if $L(t)$ is greater than a pre-defined threshold. By using the method in [16], we show in Appendix A that the evolution of the log-probability ratio $L(t)$ obeys the following ODE:

$$\frac{dL(t)}{dt} = \left[\frac{dX_*(t)}{dt} \right]_+ \log \left(\frac{J_1(t_-)}{J_0(t_-)} \right) - k_0 (J_1(t) - J_0(t)) \quad (4)$$

where $[w]_+ = \max(w, 0)$. The quantity $J_s(t) = \mathbf{E}\{\{XK\}(t)|s, \mathcal{X}_*(t)\}$ is the posteriori mean of the number of XK molecules at time t given the history $\mathcal{X}_*(t)$ and the assumption that the transmitter has sent Symbol s . We can determine $J_s(t)$ by solving an optimal Bayesian filtering problem [39]. We assume that the two transmission symbols are equally likely so $L(0) = 0$.

The MAP demodulator is located in the back-end of the receiver in Fig. 1. In the next section, we will show that it is possible to use enzymatic cycles to approximately realize the ODE in (4) and hence the back-end.

IV. DESIGNING AN ENZYMATICAL CYCLE-BASED RECEIVER

In this section, we use enzymatic cycles as the circuit components to realise a receiver that can approximately compute the log-posteriori probability in ODE (4). The overall

receiver design consists of three enzymatic cycles. One cycle is used in the front-end while the other two are used in the back-end. Our design starts with imposing the requirements that the front-end, whose reactions are given in (2), should have a high input impedance and high sensitivity. We show in Sec. IV-A how the rate parameters in (2) can be chosen to have these properties. We next move onto designing the back-end which is to realise (4) using enzymatic cycles. This consists of two steps. The first step, which is in Sec. IV-B, is to derive an approximation of (4) which removes the computational demanding parts of (4). We then show in Sec. IV-C how we can use enzymatic cycles to realise the approximation of (4) that we have derived in Sec. IV-B.

A. Parameters of receiver front-end

As discussed in Sec. III-B, we can view the receiver front-end as a device that measures the number of signalling molecules K in the receiver voxel. We will show that we can make the front-end enzymatic cycle to have a high input impedance and be sensitive to the count of K by using suitable choice of rate parameters.

Our method of achieving the desirable properties of the front-end enzymatic cycle (2) is to make use of time-scale separation. Of the four reaction rate constants in (2), we assume that d_0 and g_0 have the largest values, followed by g_- and all these three rate constants are much greater than a_0 . In other words, the forward reaction in (2a) is the slowest, while the other three reactions in (2) are faster.

In Appendix B, we use quasi-steady analysis [35] to show that:

$$[XK](t) = [X]_T \frac{[K](t)}{H_{M0} + (1 + \gamma)[K](t)} \quad (5)$$

$$[X_*](t) = [X]_T \frac{\gamma[K](t)}{H_{M0} + (1 + \gamma)[K](t)} \quad (6)$$

where $H_{M0} = \frac{d_0 + g_0}{a_0}$ and $\gamma = \frac{g_0}{g_-}$. (Note that H_{M0} is known as a Michaelis-Menten constant in the chemistry literature, hence the subscript “M”.) Since we assume that $d_0, g_0 > g_- \gg a_0$, therefore $H_{M0} \gg 1$ and $\gamma > 1$. If we choose the rate constants so that $H_{M0} \gg [K](t)$ while ensuring that γ is not too large, we see from (5) that the number of XK molecules is small.

Let us first recall that XK is a complex formed by the binding of a K molecule to an X molecule. Once a K molecule has been bound to an X molecule to form an XK molecule, this K molecule can no longer be used as it is sequestered with an X. Since XK is the only molecule in the front-end (2) that sequesters the signalling molecule K, so a small XK means the front-end “draws” only a small number of K molecules in order to perform its measurements. This is analogous to a voltmeter drawing only a small current because it is designed to have high impedance. We can ensure that the enzymatic cycle (2) has a high input impedance by requiring $H_{M0} \gg [K](t)$ holds for both Symbols 0 and 1. Given that $[K](t)$ is higher for Symbol 1 and $[K](t)$

is highest at steady state, therefore $H_{M0} \gg [K]_1^{ss}$ is the requirement for the front-end to have high input impedance.

We can view $X_*(t)$ as the output of the receiver front-end. Ideally, we want the two symbols to produce very different amount of X_* to enable the back-end to distinguish between the two symbols. We therefore use $[X_*]_1^{ss} - [X_*]_0^{ss}$ as a sensitivity measure of the front-end. We show in Appendix B that there is a $\gamma > 1$ that maximises the difference $[X_*]_1^{ss} - [X_*]_0^{ss}$. Overall, this means we can make the front-end to have both high sensitivity and input impedance by suitably choosing the its kinetic parameters.

Note that the arguments in this section and Appendix B is based on deterministic chemical rate equations. We will use stochastic simulation in Sec. V to show that the number of XK molecules is small for the stochastic case.

We have now discussed how the parameters of the front-end enzymatic cycle can be chosen. In the next sub-section, we will explain how we can turn (4) into a form which can be realised by enzymatic cycles.

B. Approximating (4)

The ODE (4) is not in a form that can be readily realised by enzymatic cycles because it contains complex mathematical operations. In this section we will use a few approximation steps to turn (4) into a form which can be realised by an enzymatic circuit in Sec. IV-C.

In the first step, we replace the posteriori mean $J_s(t) = E[\{XK\}(t)|s, \mathcal{X}_*(t)]$ in (4) by a closed-form approximation. In Appendix C, we show that if $H_{M0} \gg [K]_1^{ss}$, which is the same assumption needed for the receiver front-end to have high input impedance, then $J_s(t)$ can be approximated by:

$$J_s(t) \approx \frac{[K]_s^{ss}}{\underbrace{\alpha_{RX,RX} g_1 \frac{X_T - X_{*,s}^{ss}}{\Omega} + [K]_s^{ss} + H_{M0}}_{\kappa_s}} (X_T - X_*(t)) \quad (7)$$

where $X_{*,s}^{ss}$ is the steady-state mean number of X_* molecules when the transmitter sends Symbol s . The quantity $\alpha_{RX,RX}$ denotes the steady state mean number of signalling molecules in the receiver voxel if signalling molecules are injected into the receiver voxel at unit rate; this quantity depends only on the parameters in the medium. Note that κ_s depends only on the transmitter, medium and front-end parameters, so it is independent of the measurements $X_*(t)$.

After substituting (7) into (4), we have:

$$\frac{dL(t)}{dt} = \left[\frac{dX_*(t)}{dt} \right]_+ \log \left(\frac{\kappa_1}{\kappa_0} \right) - k_0 (\kappa_1 - \kappa_0) (X_T - X_*(t)) \quad (8)$$

The above ODE is still difficult to realise by chemical reactions. In particular, the existing methods to implement derivatives [40] and subtraction [41] (or specifically the subtraction in $(X_T - X_*(t))$) require additional chemical species and reactions to be introduced. In Appendix D, we

show that, if the receiver front-end has high input impedance, then we can approximately compute $L(t)$ in (8) by using:

$$\frac{dL(t)}{dt} \approx g_- X_*(t) \left[\log \left(\frac{\kappa_1}{\kappa_0} \right) - H_{M0} \Omega \frac{\kappa_1 - \kappa_0}{K(t)} \right] \quad (9)$$

which is free of the derivative and the subtraction $(X_T - X_*(t))$.

However, $L(t)$ in (9) is still difficult to realise by chemical reactions because $L(t)$ can be positive and negative numbers. The existing method to implement chemical-based computation system that uses both positive and negative numbers is complex because such systems need more chemical species and reactions [41][42]. Our proposal to overcome this problem is the same as that in our earlier work [43] [9] which is to avoid computing the negative $L(t)$. Our proposal is to compute an approximation $\hat{L}(t)$ which has the properties:

- $\hat{L}(t) \approx L(t)$ when the transmitter sends Symbol 1; and,
- $\hat{L}(t) \approx 0$ when the transmitter sends Symbol 0.

Since $L(t)$ is positive with a high probability if the transmitter sends a Symbol 1, this means that $\hat{L}(t)$ is highly likely to be positive when Symbol 1 is sent; and, by the above construction, $\hat{L}(t)$ is 0 when Symbol 0 is sent. Therefore, we can use $\hat{L}(t)$ together with a positive threshold to differentiate whether the transmitter sends a 0 or 1. Our proposal to obtain $\hat{L}(t)$ is to apply the $[\]_+$ operator to both sides of (9) to obtain:

$$\frac{d\hat{L}(t)}{dt} = g_- X_*(t) \underbrace{\left[\log \left(\frac{\kappa_1}{\kappa_0} \right) - H_{M0} \Omega \frac{\kappa_1 - \kappa_0}{K(t)} \right]_+}_{\text{Threshold-hyperbolic function } \phi(K(t))} \quad (10)$$

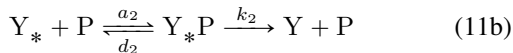
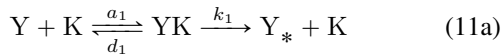
where $\hat{L}(0) = 0$. It can readily be seen that $\hat{L}(t) \geq 0 \forall t \geq 0$. The threshold-hyperbolic (TH) function in (10) has the property that if $K(t) \leq H_{M0} \Omega (\kappa_1 - \kappa_0) / \log \left(\frac{\kappa_1}{\kappa_0} \right)$, then $\hat{L}(t) = 0$. Intuitively, if the transmitter sends a Symbol 0, then the number of signalling molecules $K(t)$ in the receiver voxel is low and consequently the TH function is zero and $\hat{L}(t) = 0$. In the contrary, if the transmitter sends a Symbol 1, $K(t)$ is large and we have $\hat{L}(t) > 0$. We will discuss in Sec. IV-C how (10) can be realised by an enzymatic circuit. In particular, we will make use of the fact that an enzymatic cycle with appropriate rate constants can be used to realise a threshold-hyperbolic function.

C. An enzymatic circuit that approximately calculates log-likelihood ratio

In this section, we will explain how an enzymatic circuit can be used to approximately compute $\hat{L}(t)$ in (10). This circuit is located in the receiver voxel. We can see from (10) that the computation of $\hat{L}(t)$ requires $X_*(t)$, which comes from the receiver front-end, and $K(t)$ which is the number of signalling molecules in the receiver voxel at time t . In particular, the quantity $K(t)$ is used to compute the TH function in (10). We will divide our explanation into 3 parts:

(i) Using an enzymatic cycle to realise the TH function in (10); (ii) Computing the RHS of (10); and (iii) Computing the integration in (10).

1) *Realising the threshold-hyperbolic function:* Our aim is to show how we can use an enzymatic cycle to realise the TH function in (10) which is a function of $K(t)$. We propose to use the following enzymatic cycle, which will be referred to as the TH-cycle, to realise the TH function:



where K is again to be interpreted as the signalling molecules in the receiver voxel whose count at time t is given by $K(t)$. The reactions in (11a) are similar to those in (2a) and (2b) except that the TH-cycle has a different substrate Y. The reactions in (11a) can be used to switch Y to its active state Y_* , whereas those in (11b) can be used to revert Y_* to Y. If (11b) is to be interpreted as a dephosphorylation reaction, then P is a phosphatase, Y_* is the phosphorylated (or active) form, and Y_*P is a complex. The quantities a_1 etc. are reaction rate constants. Let $H_{M1} = \frac{d_1 + g_1}{a_1}$ and $H_{M2} = \frac{d_2 + g_2}{a_2}$ be the Michaelis-Menten constants of the TH-cycle.

We assume that the species Y, YK, Y_* , P and Y_*P are only found in the receiver voxel and they stay within the voxel. Since the signalling molecule K can bind to X in the front-end (which is also located in the receiver voxel) as well as to Y in the TH-cycle, so the species X and Y compete for K in the receiver voxel. Here, we will analyse the TH-cycle assuming that the front-end (2) is not present. We will consider the interaction of the front-end and the TH-cycle in Sec. IV-C2.

The P molecule can exist in its free form P or in the complex Y_*P , so the sum of the counts of free form P and complex Y_*P is a constant, and we will denote it by P_T . Similarly, the total count of Y in its various forms is denoted by Y_T .

Since the TH-cycle has multiple non-linearities, we carry out a simplified analysis which assumes that the total number of K molecules in the receiver voxel is a constant value denoted by K_T . We will justify this simplification later on using time-scale separation.

In Appendix E, we analyse how the steady-state count of Y_* , which is the “output” of TH-cycle (11), depends on K_T . Under the assumption that $H_{M1} \gg \frac{K_T}{\Omega}$, $H_{M2} \ll \frac{P_T}{\Omega}$ and sufficiently large $\frac{k_1 K_T}{k_2 P_T}$, we show in Appendix E using the results in [44] that the steady state number of Y_* molecules can be approximated by the following TH function:

$$Y_* \approx \begin{cases} 0 & \text{for } K_T < \frac{h_1 \Omega}{h_0} \\ h_0 - \frac{h_1 \Omega}{K_T} & \text{for } K_T > \frac{h_1 \Omega}{h_0} \end{cases} \quad (12)$$

where $h_0 = Y_T - (1 + \frac{k_2}{k_1})P_T$ and $h_1 = \frac{k_2}{k_1}P_T H_{M1}$. This shows that we can use the steady state number of Y_* molecules to realise a TH function of K_T .

We note in particular that a requirement for the TH-cycle (11) to behave as a TH-function is $H_{M1} \gg \frac{K_T}{\Omega}$, which means H_{M1} has to be chosen so that it is much higher than the concentration of the K molecules in the receiver voxel. This is the same as requiring that the TH-cycle (11) to have high input impedance and a consequence is that few K molecules will be sequestered by the TH cycle.

We explain in Appendix F how we can find reaction rate constants (a_1 , d_1 , etc) for the TH-cycle such that the number of Y_* molecules is proportional to the TH function in (10). Note that the choice of the rate constants has to make $H_{M1} \gg \frac{K_T}{\Omega}$, $H_{M2} \ll \frac{P_T}{\Omega}$, which are required for the cycle in (11) to behave as a TH-function. In particular, given that we $H_{M1} = \frac{d_1 + g_1}{a_1}$ has to be large. This can be achieved by having a small a_1 which implies that the reaction $Y + K \rightarrow YK$ is slow. We learn from the slow-scale tau-leaping algorithm [45] that this reaction is then driven by the average number of K molecules. At the same time, the calculation of the TH-function by (12) is based on the steady state. Overall, this means the calculation of the TH-function by the TH-cycle (11) is driven by the steady state mean number of $K(t)$. This justifies why we could use a constant K_T for an approximate analysis in Appendix E.

2) *Computing the RHS of (10):* In this section, we will explain how we can compute the RHS of (10).

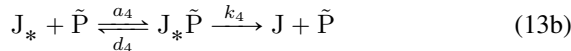
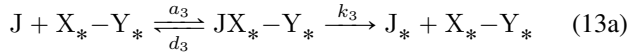
We first address the issue that both the receiver front-end (with substrate X) and the TH-cycle (with substrate Y) compete for signalling molecule K in the receiver voxel to produce the active form X_* and Y_* in their respective cycle. So far, we have analysed the front-end and the TH-cycle separately in Sec. IV-A and IV-C1, without considering the competition for K between these cycles. As an illustration of this competition, let us assume that some K molecules have been bound to form XK in the front-end, then these K molecules are no longer available for binding with Y in the TH-cycle and this means the TH-cycle “sees” a reduced number of K molecules. Fortunately, both the front-end and the TH-cycle have high impedance because $H_{M0}, H_{M1} \gg \frac{K_T^{ss}}{\Omega}$. This implies that very few K molecules are sequestered in XK and YK. Therefore, we can justify the derivations earlier where we analyse the front-end and the TH-cycle separately.

We now explain how the RHS of (10) can be computed. From the design of the TH-cycle, we can make the TH-function in (10) to be proportional to $Y_*(t)$, so the RHS of (10) is proportional to the product $X_*(t)Y_*(t)$. We propose to realise this product by using a molecule that has two binding sites to which the signalling molecule K can bind. We use the symbol X–Y to denote the structure of this molecule where the X part of the molecule behaves like the X in the front-end (2) and similarly the Y part behaves as the Y in the TH-cycle (11). The molecule X–Y can have numerous states, e.g., X–Y (where both X and Y are inactive), X_*-Y , $X-Y_*$, X_*-Y_* (where both X and Y are active) etc. With the assumption that the probabilities of X and Y being activated by K are independent, we show in Appendix G that the product

$X_*(t)Y_*(t)$ is proportional to the number of molecules in the X_*-Y_* state. Therefore, a scaled version of $\hat{L}(t)$ in (10) can be obtained from integrating the number of molecules in X_*-Y_* state over time. As a remark, we want to point out that there are many examples of protein molecules that have multiple binding sites. For example, if the binding results in phosphorylation, then these types of molecules are studied under the topic of multi-site phosphorylation [46]. We also note that independent binding assumption is also used in a lot of analysis in multi-site phosphorylation [47]; this justifies the use of independent binding assumption earlier.

We have so far not discussed the time-scale for the reactions in the enzymatic cycles for X and Y. We see from our earlier analysis that the TH-function calculation in (12) requires the TH-cycle to reach the steady state. This means that only the steady state portion of the TH-cycle signal is useful; this also holds for the receiver front-end. Therefore, in order to achieve accurate detection, we will need the integration time for computing $\hat{L}(t)$ to be long compared to the time-scale for the two enzymatic cycles for X and Y to reach the steady state. In other words, both enzymatic cycles should have a short transient compared with the symbol duration.

3) *Computing the integration in (10)*: In this paper, we will use an enzymatic cycle to realise the integration in (10). We assume that X_*-Y_* reacts with a substrate J in the following enzymatic cycle:



Our aim is to ensure that the number of J_* molecules is proportional to the integral $\int_0^t \{X_* - Y_*\}(\tau) d\tau$ and therefore proportional to $\hat{L}(t)$. We achieve this by using large Michaelis-Menten constants $K_{M3} = \frac{d_3+k_3}{a_3}$ and $K_{M4} = \frac{d_4+k_4}{a_4}$ in both directions of the cycle and to ensure that the cycle operates far away from saturation. The use of a large Michaelis-Menten constant for the forward path (13a) of the cycle also ensures that few X_*-Y_* are sequestered. Since the design of the integrator is not a key purpose of this paper, we will not delve into further details.

4) *Enzymatic receiver circuit*: We have now completed the description of the three enzymatic cycles — front-end (2), TH-cycle (11) and integrator (13) — which work together to compute the approximate log-probability ratio $\hat{L}(t)$. These three cycles together form an enzymatic cycle-based receiver. We will use the term *enzymatic receiver* to refer to the receiver formed by these 3 cycles.

V. NUMERICAL EVALUATIONS

The aim of this section is to use numerical experiments to understand the properties of the proposed enzymatic receiver. We first describe the experimental settings.

A. Experimental settings

We consider a medium of $2\mu\text{m} \times 2\mu\text{m} \times 1\mu\text{m}$. We assume a voxel size of $W^3 \mu\text{m}^3$ where $W = \frac{1}{3}$, creating an array of $6 \times 6 \times 3$ voxels. The voxel coordinates for the transmitter and receiver are, respectively, (2,3,2) and (5,3,2). We assume the diffusion coefficient D of the medium is $1 \mu\text{m}^2\text{s}^{-1}$. We assume an absorbing boundary for the medium and the signalling molecules escape from a boundary voxel surface at a rate of $\frac{D}{50W^2}$. These values are the same as those used in the earlier study [8].

We assume that the transmitter uses the reaction (1) to produce the signalling molecules. We will use two different transmitter parameter settings. The first setting will result in steady state mean counts of 12 and 40 signalling molecules in the receiver voxel when Symbols 0 and 1 are transmitted. In contrast, *TX-setting-2* will result in 4 and 12 signalling molecules at the receiver voxel. Appendix H contains the transmitter parameter values that will result in these signalling molecule counts in the receiver voxel. Furthermore, we assume that the symbol duration is 30s.

The parameters of the receiver front-end have been chosen to satisfy $d_0, g_0 > g_- \gg a_0$ (see Sec. IV-A) so that its input impedance is high. We used $a_0 = 10^{-3}$, $d_0 = g_0 = 20$ and $g_- = 1$. The number of $X-Y$ molecules is chosen to be 37; this is comparable to the number of receptors used in [8]. We use the algorithm in Appendix F (which is discussed in Sec. IV-C) to calculate the parameters of the TH-cycle. We put the value of the calculated TH-cycle parameters, as well as those of the integrator, in Appendix H.

All the simulations are carried out by using the Stochastic Simulation Algorithm (SSA) [48].

B. Input impedance and front-end signal

We first demonstrate that our parameter choice for the front-end will result in a small count of XK which means only a small number of signalling molecules K is sequestered. Fig. 2 shows the counts of XK molecules (blue curve) for one SSA realisation when Symbol 0 or Symbol 1 is sent. The red curve show the solution of the ODEs obtained from writing down the reaction-rate equations of the system and these curves show approximately the average counts. In order to show that the XK counts are low, we compare them to the counts of X_* which are plotted in Fig. 3. We can see that at steady state for Symbol 1, the counts of X_* molecules fluctuate around of a mean of about 12 molecules but the counts XK molecules stay around 1 or 2 mostly. Thus, the number of XK molecules remain low for Symbol 1; the same applies to Symbol 0.

C. Filtering approximation

The aim of this section is to verify the accuracy of the closed-form formula (7) that approximately computes the posteriori mean $E[\{XK\}(t)|s, \mathcal{X}_*(t)]$ of the number of XK molecules. The exact numerical computation of the posteriori

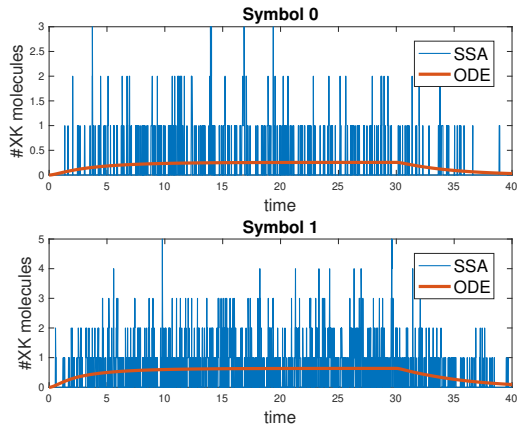


Fig. 2: Number of XK molecules for Symbol 0 and 1. These results are for *TX-setting-1*.

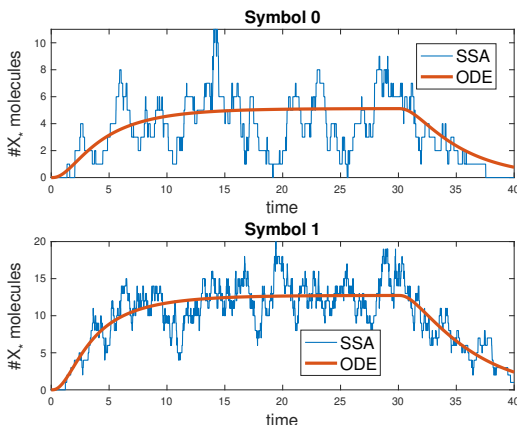


Fig. 3: Number of X_* molecules for Symbol 0 and 1. These results are for *TX-setting-1*.

mean is demanding because we need to compute the time evolution of the probabilities of the all the states that are compatible with the given observations $\mathcal{X}_*(t)$. We are unable to do that with the medium specified in Sec. V-A because the number of states will be more than 10^{200} if we assume each voxel has no more than 100 signalling molecules. We therefore need to use a smaller medium for this verification. We have chosen to use a medium which consists of one voxel, which means the transmitter and receiver are co-located at the same voxel. We will need to calculate the evolution of approximately 2500 state probabilities which means solving 2500 ODEs of the same number of variables. If we add another voxel, the number of states needed will jump by 10^2 folds so the computation demand is again high.

We use the 1-voxel medium, *TX-setting-1* and the receiver front-end parameters together with SSA algorithm to simulate the system. We use the system model and the observations $\mathcal{X}_*(t)$ to compute the exact posteriori mean and its closed-form approximation. Fig. 4 shows the results for both Symbols 0 and 1. It can be seen that the approximation is accurate except for the initial transient. This is because the

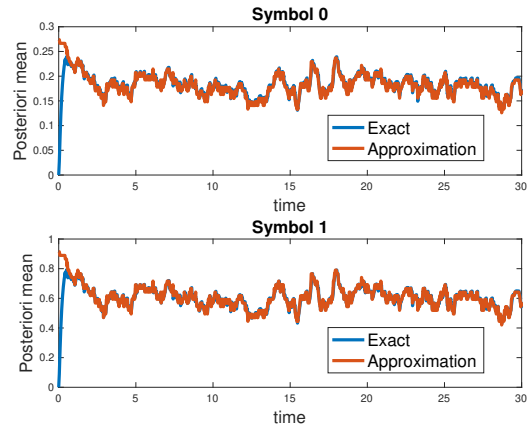


Fig. 4: The exact posteriori mean $J_s(t) = E[\{XK\}(t)|s, \mathcal{X}_*(t)]$ and its approximation is (7).

approximation assumes that the system is in steady state so it cannot deal with the transient.

D. Log-probability approximation - small medium

The aim of this section is to demonstrate that the approximate log-probability ratio computed by (8) and (10) are accurate. We compare these approximations against the exact log-probability ratio $L(t)$ in (4). Since the numerical calculation of the exact $L(t)$ requires the solution of a Bayesian filtering problem, so the comparison here is based on the small medium that we use in Sec. V-C.

Fig. 5 compares, for Symbol 1, one realisation of the exact log-probability ratio $L(t)$ (in black solid line) and its approximation (8) (in red solid line) and (10) (in blue solid line). The approximation (8) is very accurate as the red line sits almost on top of the black line. We further compute the root-mean-square error (RMSE) of the two approximations over 200 realisations. The results are plotted as dash lines in Fig. 5. We can see that both approximations have small RMSEs.

Fig. 6 shows similar comparisons but this time for Symbol 0. The approximation (8) (in red solid line) is again very accurate. For Symbol 0, the approximation (10) is 0 as shown by the blue solid line in the figure.

Since we have shown that (8) is an accurate approximation of the exact $L(t)$ and we are unable to compute the exact $L(t)$ for large medium, we will use (8) as the correct $L(t)$ for the larger medium defined in Sec. V-A. From this point onwards, the results will be based on the larger medium.

E. Log-probability ratio computed by an enzymatic receiver

The aim of this section is to show that the output of the enzymatic receiver is approximately equal to the log-probability ratio when Symbol 1 is sent and is almost 0 when Symbol 0 is sent. Fig. 7 compares, for Symbol 1, a realisation of the enzymatic circuit output (red line) and that of approximate log-probability ratio (8) (blue line). It can

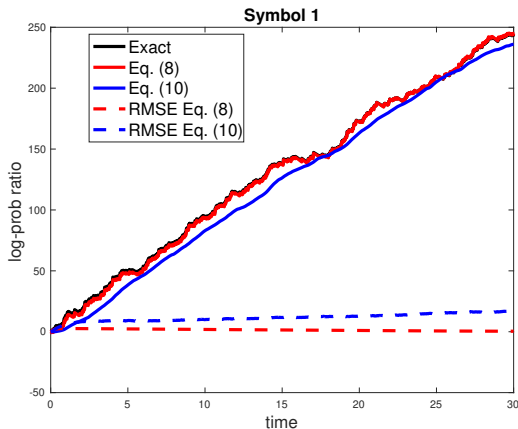


Fig. 5: One realisation of the exact log-probability ratio and its approximation (8) and (10) (solid line). RMSE between exact and the approximation (dashed lines). Symbol 1.

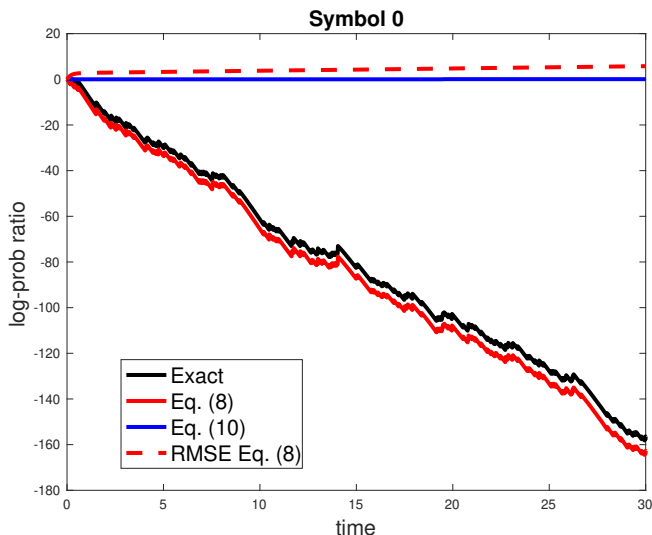


Fig. 6: One realisation of the exact log-probability ratio and its approximation (8) and (10) (solid line). RMSE between exact and the approximation (dashed lines). Symbol 0.

be seen that, after a period of transient, they become fairly close to each other. The black line in Fig. 7 shows the RMSE, over 200 realisations, between the enzymatic circuit output and (8); it can be seen that the RMSE is low. Lastly, when Symbol 0 is sent, the output of the enzymatic circuit is almost zero as shown by the magenta dashed lines in the Fig. 7.

F. Bit-error ratio and multiple receivers

This section studies the bit-error ratio (BER) of the enzymatic receiver circuit for two scenarios: one receiver and two receivers. We begin with the one receiver scenario.

The demodulation decision is based on the output of the enzymatic receiver circuit. If the output is higher than a threshold at the decision time, then the demodulator decides that Symbol 1 has been sent; otherwise it decides for Symbol

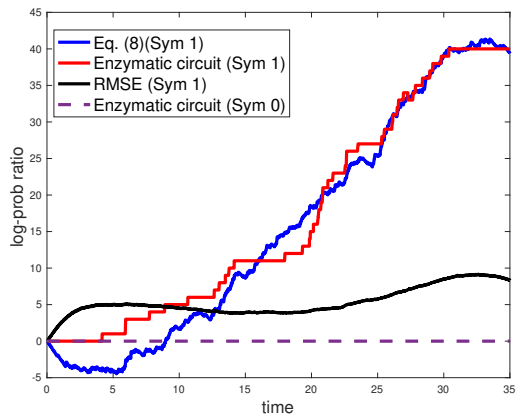


Fig. 7: Comparing the output of the enzymatic circuit against that of log-probability ratio (8).

0. In this study, we fix the decision threshold to 10 and vary the decision time from 0 to 30, which is the symbol duration. The blue line in Fig. 8 shows how the BER varies with decision time. We can see that we can achieve a small BER when the decision time is high enough. As a comparison, we use the approximate log-probability ratio (8) and the same threshold for demodulation. This can be considered as the BER achievable by using high precision digital computation. The BER for using (8) is plotted as blue dashed lines in Fig. 8. It can be seen that the enzymatic receiver requires a longer time to achieve the same BER compared to using (8). This longer time is due to time needed for the reactions to take place. This shows that the enzymatic receiver can achieve good BER provided that the decision time is long enough.

The results in the previous paragraph assumes that the medium has only one receiver located at the voxel with coordinates (5,3,2). We now consider what happens when there are two receivers in the medium where one of the receiver is still located at (5,3,2) and the other receiver is located at a different voxel. We consider two possible locations of this second receiver: (4,5,2) and (5,5,2). Fig. 8 shows the BER of the receiver at (5,3,2) when the medium has 1 or 2 receivers. It can be seen that the BER is not affected much with the presence of another receiver.

The earlier discussion is based on *TX-setting-1* which expects on average 12 and 40 signalling molecules in the receiver voxel for, respectively, Symbols 0 and 1. We now consider *TX-setting-2* which expects 4 and 12 signalling molecules in the receiver voxel for the two symbols. We plot the BER against the decision time in Fig. 9. It shows that it takes a longer time to reach the same BER because fewer signalling molecules are used. At the same time, we also can see that BER is again not affected much with the presence of another receiver. This shows that we can trade the resource requirement of communications (in terms of the number of signalling molecules being produced) against decision time.

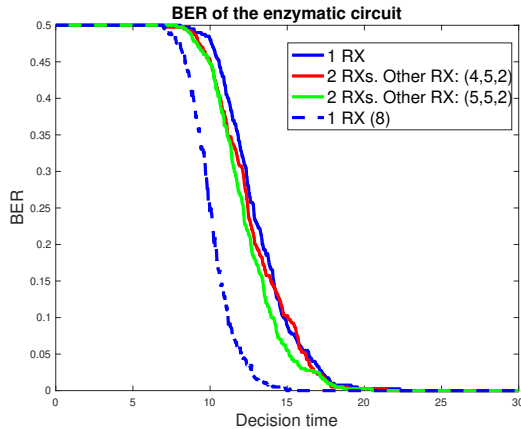


Fig. 8: Comparing the BER of the enzymatic circuit. For *TX-setting-1*.

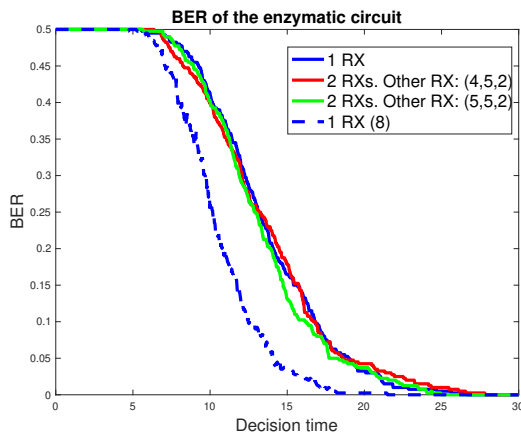


Fig. 9: Comparing the BER of the enzymatic circuit. For *TX-setting-2*.

VI. CONCLUSIONS

This paper presents a chemical reaction-based receiver that can demodulate concentration modulated signals. The receiver uses enzymatic cycles as its building block. We show how we can choose the parameters of these cycles so that this receiver has high input impedance and can approximately act as a maximum a-posteriori demodulator.

REFERENCES

- [1] I. Akyildiz, F. Brunetti, and C. Blázquez, “Nanonetworks: A new communication paradigm,” *Computer Networks*, vol. 52, pp. 2260–2279, 2008.
- [2] T. Nakano, T. Suda, Y. Okaie, M. J. Moore, and A. V. Vasilakos, “Molecular Communication Among Biological Nanomachines: A Layered Architecture and Research Issues,” *IEEE Transactions on NanoBioscience*, vol. 13, no. 3, pp. 169–197, 2014.
- [3] N. Farsad, H. B. Yilmaz, A. Eckford, C.-B. Chae, and W. Guo, “A Comprehensive Survey of Recent Advancements in Molecular Communication,” *IEEE Communications Surveys & Tutorials*, vol. 18, no. 3, pp. 1887–1919, Aug. 2016.
- [4] D. Bi, A. Almpanis, A. Noel, Y. Deng, and R. Schober, “A Survey of Molecular Communication in Cell Biology: Establishing a New Hierarchy for Interdisciplinary Applications,” *IEEE Communications Surveys & Tutorials*, vol. 23, no. 3, pp. 1494–1545, 2021.
- [5] V. Jamali, A. Ahmadzadeh, W. Wicke, A. Noel, and R. Schober, “Channel Modeling for Diffusive Molecular Communication—A Tutorial Review,” *Proceedings of the IEEE*, vol. 107, no. 7, pp. 1256–1301, 2019.
- [6] M. Femminella and G. Reali, “Implementation issues of diffusion-based molecular communications receivers based on transcriptional elements,” *Digital Signal Processing*, vol. 124, p. 103160, 2022.
- [7] M. Kuscü and O. B. Akan, “Channel Sensing in Molecular Communications With Single Type of Ligand Receptors,” *IEEE Transactions on Communications*, vol. 67, no. 10, pp. 6868–6884, 2019.
- [8] C. T. Chou, “Designing Molecular Circuits for Approximate Maximum a Posteriori Demodulation of Concentration Modulated Signals,” *IEEE Transactions on Communications*, vol. 67, no. 8, pp. 5458–5473, 07 2019.
- [9] —, “Using transcription-based detectors to emulate the behavior of sequential probability ratio-based concentration detectors,” *Physical Review E*, vol. 106, no. 5, p. 054403, 2022.
- [10] D. Bi, Y. Deng, M. Pierobon, and A. Nallanathan, “Chemical Reactions-Based Microfluidic Transmitter and Receiver Design for Molecular Communication,” *IEEE Transactions on Communications*, vol. 68, no. 9, pp. 5590–5605, 2020.
- [11] V. Walter, D. Bi, A. Salehi-Reyhani, and Y. Deng, “Real-time signal processing via chemical reactions for a microfluidic molecular communication system,” *Nature Communications*, vol. 14, no. 1, p. 7188, 2023.
- [12] B. Heinlein, L. Brand, M. Egan, M. Schäfer, R. Schober, and S. Lotter, “Stochastic Chemical Reaction Networks for MAP Detection in Cellular Receivers,” *Proceedings of the 10th ACM International Conference on Nanoscale Computing and Communication*, pp. 65–71, 2023.
- [13] B. Alberts *et al.*, *Molecular Biology of the Cell*, 5th ed. Garland Science, 2007.
- [14] X. J. Gao, L. S. Chong, M. S. Kim, and M. B. Elowitz, “Programmable protein circuits in living cells.” *Science*, vol. 361, no. 6408, pp. 1252–1258, 09 2018. [Online]. Available: <http://www.sciencemag.org/lookup/doi/10.1126/science.aat5062>
- [15] C. T. Chou, “A Markovian Approach to the Optimal Demodulation of Diffusion-Based Molecular Communication Networks,” *IEEE Transactions on Communications*, vol. 63, no. 10, pp. 3728–3743, Oct. 2015.
- [16] H. Awan and C. T. Chou, “Generalized Solution for the Demodulation of Reaction Shift Keying Signals in Molecular Communication Networks,” *IEEE Transactions on Communications*, vol. 65, no. 2, pp. 715–727, Feb. 2017.
- [17] B. D. Unluturk, A. O. Bicen, and I. F. Akyildiz, “Genetically Engineered Bacteria-Based BioTransceivers for Molecular Communication,” *IEEE Transactions on Communications*, vol. 63, no. 4, pp. 1271–1281, Apr. 2015.
- [18] M. Pierobon, “A systems-theoretic model of a biological circuit for molecular communication in nanonetworks,” *Nano Communication Networks*, vol. 5, no. 1-2, pp. 25–34, May 2014.
- [19] M. Kuscü and O. B. Akan, “Maximum Likelihood Detection With Ligand Receptors for Diffusion-Based Molecular Communications in Internet of Bio-Nano Things,” *IEEE Transactions on Nanobioscience*, vol. 17, no. 1, pp. 44–54, Mar. 2018.
- [20] M. Egan, T. Q. Duong, and M. D. Renzo, “Biological Circuits for Detection in MoSK-Based Molecular Communication,” *IEEE Access*, vol. 7, pp. 21 094–21 102, 2019.
- [21] H. Awan and C. T. Chou, “Improving the Capacity of Molecular Communication Using Enzymatic Reaction Cycles,” *IEEE Transactions on Nanobioscience*, vol. 16, no. 8, pp. 744–754, 01 2018. [Online]. Available: <http://ieeexplore.ieee.org/document/8039237/>
- [22] F. Ratti, M. Magarini, and D. D. Vecchio, “What Is the Trait d’Union between Retroactivity and Molecular Communication Performance Limits?” *Molecules*, vol. 27, no. 10, p. 3130, 2022.
- [23] A. Marcone, M. Pierobon, and M. Magarini, “A parity check analog decoder for molecular communication based on biological circuits.” *INFOCOM*, 2017.
- [24] —, “Parity-Check Coding Based on Genetic Circuits for Engineered Molecular Communication Between Biological Cells,” *IEEE Transactions on Communications*, vol. 66, no. 12, pp. 6221–6236, Dec. 2018.
- [25] A. Lombardo, G. Morabito, C. Panarello, and F. Pappalardo, “Inter-cellular Chemical Communication Through EV Exchange: Evaluation of the EV Fusion Process Parameters at the Receiving Cell,” *IEEE*

- Transactions on Molecular, Biological, and Multi-Scale Communications*, vol. 10, no. 1, pp. 21–31, 2024.
- [26] M. Veletić, M. T. Barros, H. Arjmandi, S. Balasubramaniam, and I. Balasingham, “Modeling of Modulated Exosome Release From Differentiated Induced Neural Stem Cells for Targeted Drug Delivery,” *IEEE Transactions on NanoBioscience*, vol. 19, no. 3, pp. 357–367, 2020.
- [27] Y. Deng, M. Pierobon, and A. Nallanathan, “A Microfluidic Feed Forward Loop Pulse Generator for Molecular Communication,” *GLOBECOM*, 2017.
- [28] H. Arjmandi, A. Ahmadzadeh, R. Schober, and M. Nasiri-Kenari, “Ion Channel Based Bio-Synthetic Modulator for Diffusive Molecular Communication,” *IEEE Transactions on Nanobioscience*, vol. 15, no. 5, pp. 418 – 432, 2016. [Online]. Available: <http://ieeexplore.ieee.org/document/7457689/>
- [29] M. Farahnak-Ghazani, G. Aminian, M. Mirmohseni, A. Gohari, and M. Nasiri-Kenari, “On Medium Chemical Reaction in Diffusion-Based Molecular Communication: A Two-Way Relaying Example,” *IEEE Transactions on Communications*, vol. 67, no. 2, pp. 1117–1132, 2019.
- [30] C. T. Chou, “Extended Master Equation Models for Molecular Communication Networks,” *IEEE Transactions on NanoBioscience*, vol. 12, no. 2, pp. 79–92, 2013.
- [31] F. Vakiliipoor, A. N. M. Ansari, M. Magarini, and F. Vakiliipoor, “Heuristic Barycenter Modeling of Fully Absorbing Receivers in Diffusive Molecular Communication Channels,” *IEEE Transactions on Communications*, vol. 72, no. 1, pp. 133–145, 2024.
- [32] C. McBride, R. Shah, and D. D. Vecchio, “The Effect of Loads in Molecular Communications,” *Proceedings of the IEEE*, vol. PP, no. 99, pp. 1 – 18, 05 2019.
- [33] C. T. Chou, “Maximum a-posteriori decoding for diffusion-based molecular communication using analog filters,” *IEEE Transactions on Nanotechnology*, vol. 14, no. 6, pp. 1054–1067, 2015.
- [34] M. U. Riaz, A. Hamdan, and C. T. Chou, “Using Spatial Partitioning to Reduce the Bit Error Rate of Diffusion-Based Molecular Communications,” *IEEE Transactions on Communications*, vol. 68, no. 4, pp. 2204 – 2220, 03 2020. [Online]. Available: <https://ieeexplore.ieee.org/document/8970546/>
- [35] C. A. Gomez-Uribe, G. C. Verghese, and L. Mirny, “Operating Regimes of Signaling Cycles: Statics, Dynamics, and Noise Filtering,” *PLoS Computational Biology*, vol. preprint, no. 2007, p. e246, 00 2005. [Online]. Available: <http://dx.plos.org/10.1371/journal.pcbi.0030246>
- [36] R. Erban, J. Chapman, and P. Maini, “A practical guide to stochastic simulations of reaction-diffusion processes,” *arXiv preprint arXiv:0704.1908*, 2007.
- [37] D. Del Vecchio and R. M. Murray, *Biomolecular Feedback Systems*. Princeton University Press, 2014.
- [38] C. Gardiner, *Stochastic methods*. Berlin, Germany: Springer, 2010.
- [39] S. Särkkä, Ed., *Bayesian filtering and smoothing*, 2nd ed. Cambridge University Press, 2013.
- [40] E. Alexis, C. C. Schulte, L. Cardelli, and A. Papachristodoulou, “Biomolecular mechanisms for signal differentiation,” *iScience*, vol. 24, no. 12, p. 103462, 2021.
- [41] K. Oishi and E. Klavins, “Biomolecular implementation of linear I/O systems,” *Systems Biology, IET*, vol. 5, no. 4, pp. 252–260, Jul. 2011.
- [42] C. T. Chou, “Chemical reaction networks for computing logarithm,” *Synthetic Biology*, vol. 2, no. 1, pp. 1–13, Apr. 2017.
- [43] —, “Detection of persistent signals and its relation to coherent feed-forward loops,” *Royal Society Open Science*, vol. 5, no. 11, Nov. 2018.
- [44] R. Straube, “Operating regimes of covalent modification cycles at high enzyme concentrations,” *Journal of theoretical biology*, vol. 431, pp. 39 – 48, 10 2017. [Online]. Available: <http://dx.doi.org/10.1016/j.jtbi.2017.08.006>
- [45] Y. Cao, D. T. Gillespie, and L. R. Petzold, “The slow-scale stochastic simulation algorithm,” *The Journal of Chemical Physics*, vol. 122, no. 1, pp. 014 116 – 19, 01 2005. [Online]. Available: <http://aip.scitation.org/doi/10.1063/1.1824902>
- [46] C. Salazar and T. Höfer, “Multisite protein phosphorylation - from molecular mechanisms to kinetic models,” *FEBS Journal*, vol. 276, no. 12, pp. 3177 – 3198, 06 2009. [Online]. Available: <http://doi.wiley.com/10.1111/j.1742-4658.2009.07027.x>
- [47] —, “Versatile regulation of multisite protein phosphorylation by the order of phosphate processing and protein-protein interactions,” *The FEBS Journal*, vol. 274, no. 4, pp. 1046 – 1061, 01 2007. [Online]. Available: <http://doi.wiley.com/10.1111/j.1742-4658.2007.05653.x>
- [48] D. Gillespie, “Exact stochastic simulation of coupled chemical reactions,” *The journal of physical chemistry*, 1977.
- [49] C. A. Gómez-Uribe, G. C. Verghese, and A. R. Tzafriiri, “Enhanced identification and exploitation of time scales for model reduction in stochastic chemical kinetics,” *The Journal of Chemical Physics*, vol. 129, no. 24, pp. 244 112 – 17, 12 2008. [Online]. Available: <http://aip.scitation.org/doi/10.1063/1.3050350>
- [50] L. Bronstein and H. Koepl, “Marginal process framework: A model reduction tool for Markov jump processes,” *Physical Review E*, vol. 97, no. 6, p. 062147, 2018.

APPENDIX A DERIVATION OF (4)

Recalling that $\mathcal{X}_*(t)$ is the history of X_* in the time interval $[0, t]$. In order to derive (4), we consider the history $\mathcal{X}_*(t + \Delta t)$ as a concatenation of $\mathcal{X}_*(t)$ and $\mathcal{X}_*(\tau)$ for $\tau \in (t, t + \Delta t]$. We assume that Δt is chosen small enough so that no more than one reaction or diffusion event can take place in $(t, t + \Delta t]$. Given this assumption and right continuity of continuous-time Markov chains, we can use $X_*(t + \Delta t)$ to denote the history of $X_*(t)$ in $(t, t + \Delta t]$.

Consider the likelihood of observing the history $\mathcal{X}_*(t + \Delta t)$ assuming that the transmitter has sent symbol s :

$$P[\mathcal{X}_*(t + \Delta t)|s] \quad (14)$$

$$= P[\mathcal{X}_*(t) \text{ AND } X_*(t + \Delta t)|s] \quad (15)$$

$$= P[\mathcal{X}_*(t)|\mathcal{H}_t] P[X_*(t + \Delta t)|s, \mathcal{X}_*(t)] \quad (16)$$

where we have expanded $\mathcal{X}_*(t + \Delta t)$ in (14) using concatenation.

By using (16) in the definition of log-probability ratio in (3), we can show that:

$$L(t + \Delta t) = L(t) + \log \left(\frac{P[X_*(t + \Delta t)|1, \mathcal{X}_*(t)]}{P[X_*(t + \Delta t)|0, \mathcal{X}_*(t)]} \right) \quad (17)$$

The conditional probability $P[X_*(t + \Delta t)|s, \mathcal{X}_*(t)]$ is the prediction of the number of X_* molecules at time $t + \Delta t$ based on its history up till time t . This conditional probability can be obtained by solving an optimal Bayesian filtering problem over the continuous-time Markov chain or RDME that describes the dynamics of the molecular network. We considered how this conditional probability could be evaluated in our earlier work [16]. The key result in [16] says that $P[X_*(t + \Delta t)|s, \mathcal{X}_*(t)]$ depends on the predicted rate of the chemical reactions in which X_* are involved. By using [16], we have:

$$\begin{aligned} &P[X_*(t + \Delta t)|s, \mathcal{X}_*(t)] = \\ &\delta_{X_*(t+\Delta t), X_*(t)+1} k_0 J_i(t_-) \Delta t + \\ &\delta_{X_*(t+\Delta t), X_*(t)-1} g_- X_*(t) \Delta t + \\ &\delta_{X_*(t+\Delta t), X_*(t)} \times \\ &(1 - k_0 J_i(t) \Delta t - g_- X_*(t) \Delta t) \end{aligned} \quad (18)$$

where $\delta_{a,b}$ is the Kronecker delta which is 1 when a equals to b and zero otherwise, and $J_i(t) = E[\{XK\}(t)|s, \mathcal{X}_*(t)]$ is the expected number of XK molecules at time t assuming that the transmitter has sent symbol s and the history $\mathcal{X}_*(t)$.

Note that $P[X_*(t + \Delta t) | s, \mathcal{X}_*(t)]$ in (18) is a sum of three terms with multipliers $\delta_{X_*(t+\Delta t), X_*(t)+1}$, $\delta_{X_*(t+\Delta t), X_*(t)-1}$ and $\delta_{X_*(t+\Delta t), X_*(t)}$. Since these multipliers are mutually exclusive, we have:

$$\begin{aligned}
& \log \left(\frac{P[X_*(t + \Delta t) | 1, \mathcal{X}_*(t)]}{P[X_*(t + \Delta t) | 0, \mathcal{X}_*(t)]} \right) \\
&= \delta_{X_*(t+\Delta t), X_*(t)+1} \log \left(\frac{k_0 J_1(t_-) \Delta t}{k_0 J_0(t_-) \Delta t} \right) + \\
& \delta_{X_*(t+\Delta t), X_*(t)-1} \log \left(\frac{g_- X_*(t) \Delta t}{g_- X_*(t) \Delta t} \right) + \\
& \delta_{X_*(t+\Delta t), X_*(t)} \times \\
& \log \left(\frac{1 - k_0 J_1(t_-) \Delta t - g_- X_*(t) \Delta t}{1 - k_0 J_0(t_-) \Delta t - g_- X_*(t) \Delta t} \right) \\
&\approx \delta_{X_*(t+\Delta t), X_*(t)+1} \log \left(\frac{J_1(t_-)}{J_0(t_-)} \right) - \\
& \delta_{X_*(t+\Delta t), X_*(t)} k_0 (J_1(t) - J_0(t)) \Delta t \quad (19)
\end{aligned}$$

where we have used the approximation $\log(1 + f \Delta t) \approx f \Delta t$ and have ignored terms of order $(\Delta t)^2$ or higher to obtain (19). Note also that the above derivation assumes that $\frac{J_1(t)}{J_0(t)}$ is strictly positive so its logarithm is well defined; this can be achieved by proper choice of the hypotheses.

By substituting (19) into (17), we have after some manipulations and after taking the limit $\Delta t \rightarrow 0$:

$$\begin{aligned}
\frac{dL(t)}{dt} &= \lim_{\Delta t \rightarrow 0} \frac{\delta_{X_*(t+\Delta t), X_*(t)+1}}{\Delta t} \log \left(\frac{J_1(t_-)}{J_0(t_-)} \right) - \\
& \delta_{X_*(t+\Delta t), X_*(t)} k_0 (J_1(t) - J_0(t)) \quad (20)
\end{aligned}$$

In order to obtain (4), we use the following reasonings. First, the term $\lim_{\Delta t \rightarrow 0} \frac{\delta_{X_*(t+\Delta t), X_*(t)+1}}{\Delta t}$ is a Dirac delta at the time instant that an X_* molecule is produced. Since the instant is also the time at which $X_*(t)$ jumps by +1, we can identify this term with $\left[\frac{dX_*(t)}{dt} \right]_+$ where $[w]_+ = \max(w, 0)$.

Since $X_*(t)$ is a piecewise constant signal counting the number of X_* molecules, its derivative is a sequence of Dirac deltas at the time instants that X is activated or X_* is deactivated. Note that the Dirac deltas corresponding to the activation of X carries a positive sign and the $[\]_+$ operator keeps only these. Fig. 10 shows an example of $X_*(t)$ and its corresponding $\left[\frac{dX_*(t)}{dt} \right]_+$.

Second, the term $\delta_{X_*(t+\Delta t), X_*(t)}$ is only zero when the number of X_* molecule changes but the number of such changes is countable. In other words, $\delta_{X_*(t+\Delta t), X_*(t)} = 1$ with probability one. This allows us to drop $\delta_{X_*(t+\Delta t), X_*(t)}$. Hence (4).

APPENDIX B DERIVATION FOR SEC. IV-A

In this appendix we use time-scale separation to understand the properties of the front-end circuit. Although there are methods for time-scale separation for chemical master equations [49], the method is not easy to apply to our case. We

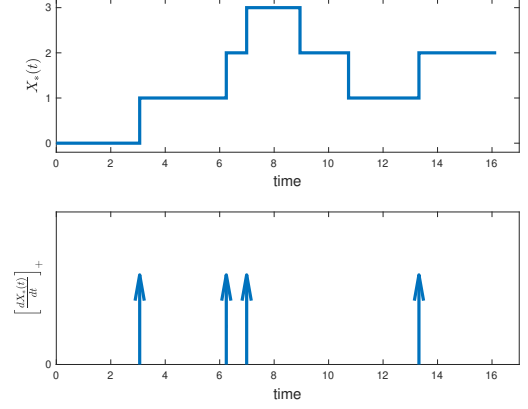


Fig. 10: The upper plot shows a sample $X_*(t)$ and the lower plot shows the corresponding $\left[\frac{dX_*(t)}{dt} \right]_+$.

have therefore chosen to use the deterministic model which is based on the reaction rate equations.

Our derivation follows the quasi-steady analysis [35] for analysing chemical reactions. Given the assumption that the reaction rate constants d_0 , g_0 and g_- are far greater than a_0 , we identify XK and X_* as fast species. The reaction rate equations for these two species are:

$$\frac{d[XK]}{dt} = a_0[K][X] - (d_0 + g_0)[XK] \quad (21)$$

$$\frac{d[X_*]}{dt} = g_0[XK] - g_-[X_*] \quad (22)$$

where we have dropped the dependence on (t) to simplify the notation. Given XK and X_* are fast species, the procedure in quasi-steady state analysis is to set their derivatives to zero. By setting the LHS of the above equations to zero and by using the conservation relation $[X] + [XK] + [X_*] = [X]_T$, we arrive at (5) and (6).

Let $[K]_s^{ss}$ be the steady state concentration of K when the transmitter sends Symbol s . By using (6), the sensitivity of the front-end can be written as:

$$\begin{aligned}
& [X_*]_1^{ss} - [X_*]_0^{ss} = \\
& \frac{\gamma [K]_1^{ss}}{H_{M0} + (1 + \gamma)[K]_1^{ss}} - \frac{\gamma [K]_0^{ss}}{H_{M0} + (1 + \gamma)[K]_0^{ss}} \quad (23)
\end{aligned}$$

We can show that the above sensitivity measure can be maximised by choosing γ to be $\frac{1}{\xi_0 \xi_1}$ where $\xi_s = \frac{[K]_s^{ss}}{H_{M0} + [K]_s^{ss}}$. It can readily be seen that we require γ to be greater than 1.

APPENDIX C APPROXIMATE BAYESIAN FILTERING

The aim of this appendix is to derive an approximation of $J_s(t) = E[\{XK\}(t) | s, \mathcal{X}_*(t)]$ whose interpretation is the posteriori mean of the number of XK molecules at time t given the hypothesis that Symbol s has been sent and the history $\mathcal{X}_*(t)$. We will derive an approximate expression for $J_s(t)$ as a function of the hypothesis s and observations $X_*(t)$. Our derivation has 2 steps. The first step uses the

product Poisson entropic matching method in [50]. In the second step, we determine a closed-form approximation of the result in the first step.

In order to simplify the presentation here, we will consider a medium consisting of 2 voxels, which we will refer to as Voxel 1 and Voxel 2. (Generalisation to the more general case is straightforward and will be explained later.) We assume that the transmitter and the receiver are located in, respectively, Voxels 1 and 2. The transmitter uses the reaction (1) to produce signalling molecules. We assume that when Symbol s is sent, the transmitter uses m_s mRNA molecules to produce signalling molecules. As in RDME, the diffusion of the signalling molecules between the voxels is modelled by a unimolecular reaction and we use \tilde{d}_i to denote its reaction rate constant. We also assume that the signalling molecules may leave the medium and we model that as a unimolecular reaction with rate constant \tilde{d}_e .

We first show how we can map our Bayesian filtering problem to the one considered in [50], which is based on reaction counts. Let $\mathcal{R}_f(t)$ (resp. $\mathcal{R}_r(t)$) be the cumulative number of times that reaction (2b) (resp. (2c)) has taken place in the time interval $[0, t]$, i.e. $\mathcal{R}_f(t)$ and $\mathcal{R}_r(t)$ are time trajectories of reaction counts. We consider the Bayesian filtering problem which uses $\mathcal{R}_f(t)$ and $\mathcal{R}_r(t)$ as the given information. We argue that we can deduce $\mathcal{R}_f(t)$ and $\mathcal{R}_r(t)$ from $\mathcal{X}_*(t)$. This is because there is only one reaction in which X_* is formed (i.e. reaction (2b)) and only one reaction in which X_* is deactivated (i.e. reaction (2c)); therefore for a given $\mathcal{X}_*(t)$, the corresponding $\mathcal{R}_f(t)$ and $\mathcal{R}_r(t)$ can be uniquely determined. Overall, this implies that we can apply the approximation method in [50] to approximate $J_s(t)$.

The Bayesian filtering problem is to use the observations $\mathcal{X}_*(t)$ and assumption s to compute the posteriori probabilities of all possible system states that are compatible with the observations. Based on the 2-voxel medium set up which we assume in this appendix, the system state $v(t)$ is the 3-tuple $(K_1(t), K_2(t), \{XK\}(t))$ where $K_i(t)$ is the number of signalling molecules in Voxel i at time t . The idea in [50] is to approximate the posteriori probability that the system is in a state by a product of independent Poisson distributions. Let $\theta_{s,1}(t)$, $\theta_{s,2}(t)$ and $\theta_{s,XK}(t)$ denote the means of three independent Poisson distributions in our problem set up. These three Poisson means are used to approximate the posteriori means, as follows: $\theta_{s,i}(t) \approx \mathbb{E}[K_i(t)|s, \mathcal{X}_*(t)]$ ($i = 1, 2$) and $\theta_{s,XK}(t) \approx \mathbb{E}[\{XK\}|s, \mathcal{X}_*(t)]$. In particular, $\theta_{s,XK}(t)$ is the approximation that we are seeking. In the following, we will drop the (t) dependence for brevity.

We now present the result of applying the method in [50] to the 2-voxel set up. The result states how the approximate posteriori means $\theta_{s,1}$, $\theta_{s,2}$ and $\theta_{s,XK}$ evolve over time. The evolution of these means consist of both discrete jumps and

continuous change. The posteriori mean $\theta_{s,XK}$ experiences a discrete jump at the time when an X_* is formed; at other times, according to [50, Eq. (33)], the evolution of $\theta_{s,i}$ and $\theta_{s,XK}$ obeys the following ODEs:

$$\frac{d\theta_{s,1}}{dt} = r_{TX}m_s - (\tilde{d}_e + \tilde{d}_i)\theta_{s,1} + \tilde{d}_i\theta_{s,2} \quad (24a)$$

$$\frac{d\theta_{s,2}}{dt} = -(\tilde{d}_e + \tilde{d}_i)\theta_{s,2} + \tilde{d}_i\theta_{s,1} - \frac{1}{\Omega}a_0\theta_{s,2}\theta_{s,X} \quad (24b)$$

$$\frac{d\theta_{s,XK}}{dt} = \frac{1}{\Omega}a_0\theta_{s,2}\theta_{s,X} - (d_0 + g_0)\theta_{s,XK} \quad (24c)$$

where $\theta_{s,X} = X_T - X_*(t) - \theta_{s,XK}$ and X_T is the total number of substrate molecules in the receiver voxel. This completes the first step which is to apply the method of [50] to our problem.

Our next step is to find an approximation for $\theta_{s,XK}$. Given the history $\mathcal{X}_*(t)$, let t_1, t_2, \dots be time instants that $\mathcal{X}_*(t)$ experiences a jump because an X_* molecule is produced or reverted. In each time interval (t_j, t_{j+1}) , the number of X_* molecules is a constant and we denote that by $X_*^{[j]}$. We note that $\theta_{s,XK}$ in (24c) is a fast variable because $d_0, g_0 \gg a_0$ so $\theta_{s,XK}$ reaches steady state quickly. Our proposal is to approximate $\theta_{s,XK}$ by a constant value in each time interval (t_j, t_{j+1}) where the constant value is the steady state solution of (24) assuming that $X_*(t)$ equals to $X_*^{[j]}$ for all $t \in [0, \infty)$. Note that our approximation for $\theta_{s,XK}$ is a piecewise constant trajectory over time and the value of the $\theta_{s,XK}$ depends on the value of $X_*^{[j]}$ and the kinetic parameters.

Our next step is to determine the steady state solution of (24) assuming that $X_*(t)$ equals to $X_*^{[j]} \forall t \in [0, \infty)$. We will use $\tilde{\theta}_{s,i}$ and $\tilde{\theta}_{s,XK}$ to denote the steady state solution of (24). By setting the LHSs of (24) to zero, we have, after some manipulations:

$$\begin{bmatrix} \tilde{\theta}_{s,1} \\ \tilde{\theta}_{s,2} \end{bmatrix} = \underbrace{\begin{bmatrix} -(\tilde{d}_i + \tilde{d}_e) & \tilde{d}_i \\ \tilde{d}_i & -(\tilde{d}_i + \tilde{d}_e) \end{bmatrix}}_{\mathcal{D}}^{-1} \begin{bmatrix} -r_{TX}m_s \\ g_1\tilde{\theta}_{s,XK} \end{bmatrix} \quad (25)$$

$$\theta_{s,XK} = \frac{1}{\Omega H_{M0}} \tilde{\theta}_{s,2} (X_T - X_*^{[j]} - \tilde{\theta}_{s,XK}) \quad (26)$$

Let $-\alpha_{RX,TX}$ and $-\alpha_{RX,RX}$ be the (2,1) and (2,2) elements of the matrix \mathcal{D}^{-1} . We can re-write the second row of (25) as:

$$\tilde{\theta}_{s,2} = \alpha_{RX,TX} r_{TX} m_s - \alpha_{RX,RX} g_1 \tilde{\theta}_{s,XK} \quad (27)$$

The constants $-\alpha_{RX,TX}$ (resp. $-\alpha_{RX,RX}$) quantify the transfer of molecules from the transmitter voxel (receiver voxel) to the receiver voxel. We can identify $\alpha_{RX,TX} r_{TX} m_s$ as the steady state mean number of K molecules in the receiver voxel, so we will denote it by K_s^{ss} which is the notation that we have used in the main text to denote such

as quantity.

By substituting the expression of $\tilde{\theta}_{s,2}$ in (27) into the RHS of (26), we can show that $\tilde{\theta}_{s,XK}$ is the smaller root of the quadratic equation $q_2x^2 + q_1x + q_0 = 0$ in the indeterminate x where the coefficients are given by:

$$q_2 = \alpha_{\text{RX,RX}} \frac{g_1}{\Omega} \quad (28)$$

$$q_1 = -(\alpha_{\text{RX,RX}} g_1 \frac{X_T - X_*^{[j]}}{\Omega} + \frac{K_s^{\text{ss}}}{\Omega} + H_{M0}) \quad (29)$$

$$q_0 = \frac{K_s^{\text{ss}}}{\Omega} (X_T - X_*^{[j]}) \quad (30)$$

Under the condition that $H_{M0} \gg \min(\alpha_{\text{RX,RX}} g_1 \frac{X_T}{\Omega}, \frac{K_s^{\text{ss}}}{\Omega})$, we can apply the approximation in [44] to show that $\tilde{\theta}_{s,XK} \approx -\frac{q_0}{q_1}$ or

$$\tilde{\theta}_{s,XK} \approx \frac{\frac{K_s^{\text{ss}}}{\Omega} (X_T - X_*^{[j]})}{\alpha_{\text{RX,RX}} g_1 \frac{X_T - X_*^{[j]}}{\Omega} + \frac{K_s^{\text{ss}}}{\Omega} + H_{M0}} \quad (31)$$

Since the term H_{M0} in the denominator is much greater than the other two terms, we will replace $X_*^{[j]}$ by the steady state mean of $X_*(t)$ assuming Symbol s is sent, which we will denote by \bar{X}_s . This is so that the denominator is independent of the observation $X_*^{[j]}$. Furthermore, the RHS of (31) is the expression for the time interval (t_j, t_{j+1}) . Since $X_*^{[j]} = X_*(t) \forall t \in (t_j, t_{j+1})$, we can therefore obtain a $\tilde{\theta}_{s,XK}$ which holds for all t by replacing $X_*^{[j]}$ in the RHS of (31) by $X_*(t)$. After that, we obtain (7) where we have used $\tilde{\theta}_{s,XK}$ as the approximation of $J_s(t)$.

Finally, we consider the condition

$$H_{M0} \gg \min(\alpha_{\text{RX,RX}} g_1 \frac{X_T}{\Omega}, \frac{K_s^{\text{ss}}}{\Omega}) \quad (32)$$

for the approximation in this Appendix to hold. The quantity $\frac{K_s^{\text{ss}}}{\Omega}$ is the concentration of the signalling molecules in the receiver voxel when the receiver is absent. We consider this quantity in Sec. IV-A and denote it by $[\bar{K}]_{s,RX}$. In Sec. IV-A, we impose the condition $H_{M0} \gg [\bar{K}]_{s,RX}$ so that the front-end molecular circuit has high input impedance. It can be shown that if $H_{M0} \gg [\bar{K}]_{s,RX}$ holds, then (32) holds. Therefore, the condition needed for high impedance is sufficient for the results in this Appendix to hold.

The derivation above assumes that there are only 2 voxels. Therefore, the matrix \mathcal{D} in (25) is 2-by-2. If there are N_v voxels, then the corresponding \mathcal{D} is a N_v -by- N_v matrix which models the diffusive movements of the signalling molecules in the medium. In this case, the vector on the RHS of (25) has 2 non-zero elements situated at the positions corresponding to the transmitter and receiver voxels. By appropriately picking out the elements in \mathcal{D}^{-1} , we will arrive at an equation of the same form as (27). Therefore, even when there are N_v voxels, the approximation for $\tilde{\theta}_{s,XK}$ has the same form as (31).

APPENDIX D DERIVATION FOR (9)

The aim of this appendix is to show that the log-probability ratio computation in (8) can be approximated by (9). We begin by writing (8) in the integral form:

$$L(T) = \int_0^T \left[\frac{dX_*(t)}{dt} \right]_+ \log \left(\frac{\kappa_1}{\kappa_0} \right) dt - k_0 (\kappa_1 - \kappa_0) \int_0^T (X_T - X_*(t)) dt \quad (33)$$

The derivation is divided into 2 steps where each step focuses on deriving an approximation for one of the integrals in (33).

Step 1: Approximating the first integral in (33)

The first integral on the RHS of (33) can be interpreted as T times the mean production rate of X_* molecules. Over a large T , we have:

$$\lim_{T \rightarrow \infty} \frac{1}{T} \int_0^T \left[\frac{dX_*(t)}{dt} \right]_+ dt = \lim_{T \rightarrow \infty} \frac{1}{T} g_0 \int_0^T \{XK\}(t) dt \quad (34)$$

where the RHS of the above equation models the production of X_* from XK according to Reaction 2b. Next, at steady state, the production rate of X_* is balanced by its reversing rate, hence we have:

$$\lim_{T \rightarrow \infty} \frac{1}{T} g_0 \int_0^T \{XK\}(t) dt = \lim_{T \rightarrow \infty} \frac{1}{T} \int_0^T g_- X_*(t) dt \quad (35)$$

By combining (34) and (35), we can therefore approximate the first integral on the RHS of (33) by:

$$\int_0^T \left[\frac{dX_*(t)}{dt} \right]_+ dt \approx \int_0^T g_- X_*(t) dt \quad (36)$$

Step 2: Approximating the second integral in (33)

We now move onto the second integral on the RHS of (33). The derivation here assumes that the system is in steady state, this allows us to replace the time average in by its ensemble average. In this part, we will overload the symbols X , X_* and $\{XK\}$ to refer to the random variables of the number of, respectively, X , X_* and XK molecules at steady state. This should not cause any confusion because the meaning should be clear from the context. With this overloading, the mean number of X at steady state is denoted by $E[X]$ etc. We first need to state or derive a number of auxiliary results.

We first need make a clarification on the notation. The reason we add a pair of curly brackets to the notation $\{XK\}$, which denotes the random variable of the number of XK molecules in steady state, is to stress that it is referring to complex XK . This is important because we will also be multiplying the random variables X and K in the derivation and we will write the multiplication as $X \cdot K$.

We will now derive or present a number of auxiliary results. After that we will combine all these auxiliary results to arrive at an approximation for the second integral in (33).

(Auxiliary Result 1) At steady state, the production and reversion of the XK molecules balance out, therefore, we have:

$$\frac{a_0}{\Omega} E[X \cdot K] = (d_0 + g_0) E[\{XK\}] \quad (37)$$

In terms of ensemble averages, we can rewrite (34) as $g_0 E[\{XK\}] = g_- E[X_*]$. By combining this with (37), we have Auxiliary Result 1:

$$E[X \cdot K] = \frac{H_{M0}\Omega}{\gamma} E[X_*] \quad (38)$$

(Auxiliary Result 2) Since the receiver front-end circuit has high input impedance, it means that we can approximate the signalling molecule count in the receiver voxel when the front-end is present by the one when the receiver is absent, we will therefore ignore the presence of the front-end for deriving this auxiliary result. Since the diffusion of the molecules is independent, the distribution of the signalling molecules in the receiver voxel is binomial. We will state a property of the approximation of the reciprocal of the mean of a binomial variable in this auxiliary result.

Consider a binomial distribution $B(Q; m, f)$ with parameters m (number of trials) and f (success probability), then for sufficiently large m and f , we have

$$\frac{1}{E[Q]} \approx E\left[I\left(\frac{1}{Q}\right)\right] \quad (39)$$

where

$$I\left(\frac{1}{q}\right) = \begin{cases} 0 & \text{for } q = 0 \\ \frac{1}{q} & \text{for } q \geq 1 \end{cases} \quad (40)$$

This result essentially says that the mean of the reciprocal of a binomial random variable (with $\frac{1}{0}$ excluded) is approximately equal to the reciprocal of the mean of the binomial random variable. If $f = 1$ and $m \geq 1$, the binomial distribution has a single outcome with a non-zero probability so (40) is exact. Intuitively, if a probability has a single modal distribution with a narrow spread, then (40) holds approximately. For $f = 0.1$, the relative error of using (40) is 3.21% for $m = 300$ and drops to 1.87% for $m = 500$. In general, the approximation is better for large m and f .

(Auxiliary Result 3) Since the forward reaction in (2a) is slow because a_0 is assumed to be small, we can show that:

$$E[(X_T - X_*) \cdot K] \approx E[X_T - X_*] E[K] \quad (41)$$

We first write $E[X \cdot K]$ as a time integral:

$$E[X \cdot K] = \int_{t=0}^{\infty} X(t)K(t)dt \quad (42)$$

The reason why we are considering this integral is because X and K are the reactants of the slow reaction in (2a). This means that the counts of X change slower than that of K. This difference in time-scale allows us to approximate the above integral.

Let t_0, t_1, \dots be a sequence of time instants at which $X(t)$ changes its value. We will re-write the integral on the RHS of (42) as a sum of integrals:

$$\int_{t=0}^{\infty} X(t)K(t)dt = \sum_{i=0}^{\infty} X(t_i) \int_{t_i}^{t_{i+1}} K(t) dt \quad (43)$$

Since $X(t)$ is slow in comparison with $K(t)$, this means the time interval $[t_i, t_{i+1})$ is likely to be long compared to the time-scale of the faster $K(t)$. This allows us to approximate the integral on the RHS of (43) by $E[K](t_{i+1} - t_i)$. Hence we have:

$$\begin{aligned} E[X \cdot K] &= \sum_{i=0}^{\infty} X(t_i) E[K] dt \\ &= E[X] E[K] \end{aligned} \quad (44)$$

Note that the above argument is identical to the one used in [45] to derive the slow-scale tau-leaping simulation algorithm.

Next, we do two substitutions. First, we note that Auxiliary Result 1 expresses $E[X \cdot K]$ in terms of $E[X_*]$. Second, we approximate $E[X]$ by $E[X_T - X_*]$ because we know the front-end circuit has high input impedance so $E[\{XK\}]$ is small. After these substitutions, we arrive at Auxiliary Result 3:

$$E[X_T - X_*] \approx \frac{H_{M0}\Omega}{\gamma} \frac{E[E_*]}{E[K]} \quad (45)$$

(Auxiliary Result 4) By using the same argument as in Auxiliary Result 3, we can show that:

$$E[X_* I\left(\frac{1}{K}\right)] \approx E[X_*] E\left[I\left(\frac{1}{K}\right)\right] \quad (46)$$

By using the above auxiliary results we have

$$\begin{aligned} &E[X_T - X_*] \\ &\approx \frac{H_{M0}\Omega}{\gamma} \frac{E[E_*]}{E[K]} \quad (\text{Aux. Result 3}) \\ &= \frac{H_{M0}\Omega}{\gamma} E[E_*] E\left[I\left(\frac{1}{K}\right)\right] \quad (\text{Aux. Result 2}) \\ &= \frac{H_{M0}\Omega}{\gamma} E[X_* I\left(\frac{1}{K}\right)] \quad (\text{Aux. Result 4}) \end{aligned} \quad (47)$$

By applying the results in the 2 steps above, we can show that (8) can be approximated by:

$$\frac{L(t)}{dt} = g_- X_*(t) \left[\log\left(\frac{\kappa_1}{\kappa_0}\right) - H_{M0}\Omega \frac{\kappa_1 - \kappa_0}{K(t)} \right] \quad (48)$$

which is (9).

APPENDIX E
DERIVING (12)

In this Appendix, we will show that the enzymatic cycle (11), which is referred to as the threshold-hyperbolic (TH) cycle in Sec. IV-C1, can be used to realise a TH function. Since the TH-cycle has multiple non-linearities, a stochastic analysis is not tractable. Instead, we will use quasi-steady state analysis [35] which is also used in Appendix B. We further simplify the analysis by not including the diffusion of K in the model. We justify this simplification by the fact that we will require the TH-cycle to have high input impedance which means few K molecules will be sequestered by this cycle. This in turn means that the behaviour of the TH-cycle can be analysed without considering the details on diffusion. Based on these simplifications, we assume that the total count of K molecules seen by the cycle is a constant and we will denote this by K_T where K_T can be considered to be the mean steady state count of signalling molecules in the receiver voxel. We expect $K_T = [K]_s^{ss}\Omega$.

We will show that under the assumptions that $H_{M1} \gg \frac{K_T}{\Omega}$, $H_{M2} \ll \frac{P_T}{\Omega}$ and $\frac{k_1 K_T}{k_2 P_T}$ is sufficiently large, then the amount of Y_* in the TH-cycle is a threshold-hyperbolic function of K_T which is the input level of the cycle.

Our derivation makes use of the results in [44] which uses quasi-steady analysis to study the properties of enzymatic cycles of the form (11). Since the quasi-steady state analysis uses concentration rather than counts, we will temporarily switch over to concentration so that the reader can better match the formulas here with those in [44]. Note that all the concentrations in this Appendix are steady state concentrations.

The implication of the assumption $H_{M2} \ll [P]_T$ has been studied in [44]. Let $\mathcal{Y} = [Y_*] + [Y_*P]$. By using [44, Eq. (29)], which holds when $H_{M2} \ll [P]_T$, we have:

$$[Y_*P] \approx \begin{cases} \mathcal{Y} \left(1 - \frac{H_{M2}}{[P]_T - \mathcal{Y}}\right) & \text{for } \mathcal{Y} < [P]_T \\ [P]_T \left(1 - \frac{H_{M2}}{\mathcal{Y} - [P]_T}\right) & \text{for } \mathcal{Y} > [P]_T \end{cases} \quad (49)$$

Since we assume H_{M2} is small, we set H_{M2} to zero in the above expressions. After some simplification, we have:

$$[Y_*] \approx 0 \quad \text{for } [Y_*] + [Y_*P] < [P]_T \quad (50)$$

$$[Y_*P] \approx [P]_T \quad \text{for } [Y_*] + [Y_*P] > [P]_T \quad (51)$$

Note that $[Y_*] + [Y_*P]$ is small when the input level is small, and vice versa. This derivation shows that if the input level is low, then according to (50) we have $[Y_*] \approx 0$ or few Y_* . This is the threshold part of the TH function. On the other hand, if the input level is high, then according to (51), we have $[Y_*P] \approx [P]_T$ or P is saturated.

We now focus on deriving an expression for $[Y_*]$ when the input is high. The assumption $H_{M1} \gg \left(1 + \frac{k_1}{k_2}\right) K_T$ implies that the following holds [44, Eq. (67)]:

$$[Y_*] + [Y_*P] = [Y]_T - \frac{[K]_T + H_{M1}}{\alpha - 1} \quad \text{for } [Y_*] + [Y_*P] > [P]_T \quad (52)$$

where $\alpha = \frac{k_1 [K]_T}{k_2 [P]_T}$. By suitable choice of the enzymatic cycle parameters, we can make $\alpha > 1$ and recall that $[Y_*P] \approx [P]_T$, therefore we have:

$$[Y_*] = \tilde{h}_0 - \frac{\tilde{h}_1}{[K]_T} \quad (53)$$

where $\tilde{h}_0 = [Y]_T - [P]_T - \frac{k_2}{k_1} [P]_T$ and $\tilde{h}_1 = \frac{k_2}{k_1} [P]_T H_{M1}$. This shows that the concentration of Y_* (i.e., $[Y_*]$) is a hyperbolic function of the input level $[K]_T$ when the input is high. The result (53) is expressed in concentration, by multiplying its both sides by Ω , we obtain (12).

APPENDIX F
PARAMETERS FOR THE TH-CYCLE

This appendix explains how we determine the rate constants of the TH-cycle (11) to realise the scaled TH function:

$$\left[\underbrace{\rho \log \left(\frac{\kappa_1}{\kappa_0} \right)}_{\zeta_0} - \underbrace{\rho H_{M0} (\kappa_1 - \kappa_0)}_{\zeta_1} \frac{\Omega}{K_T} \right]_+ \quad (54)$$

where $\rho > 0$ is a scaling constant. The value of ρ can be chosen so that the probability that Y is active is high when the number of K molecules is high. Note that if one scales the log-probability ratio (10) and the detection decision threshold by the same constant, the property of the detector does not change, therefore the scaling mentioned above is allowed.

We assume that ρ has been chosen beforehand, so we can assume ζ_0 and ζ_1 are given. In addition, as stated in Sec. IV-C2, we use molecules of the form $X \rightarrow Y$ to realise the computation of on the RHS of (10). This means that $[X]_T = [Y]_T$. Here, we assume that the concentration $[X]_T$ has been chosen and that means the concentration $[Y]_T$ has been fixed.

By comparing (54) and (53), we have:

$$[Y]_T - [P]_T - \frac{k_2}{k_1} [P]_T = \zeta_0 \quad (55)$$

$$\frac{k_2}{k_1} [P]_T H_{M1} = \zeta_1 \quad (56)$$

The Michaelis-Menten constant H_{M1} needs to be much bigger than $[K]_T$ for the cycle (11) to behave as a threshold-hyperbolic function. We arbitrarily choose H_{M1} to be 10 times larger than the maximum $[K]_T$ that the PH-cycle will encounter which happens when Symbol 1 is sent. Once H_{M1} has been fixed, the values of $\frac{k_1}{k_2}$ and $[P]_T$ can be

solved from the above two equations for the given $[Y]_T$.

Since we need $[P]_T \gg H_{M2}$ for the threshold-hyperbolic behaviour, we set $H_{M2} = \frac{[P]_T}{80}$ where 80 is an arbitrary choice. As mentioned in Sec. IV-C2, we choose k_1 and k_2 so that the reaction time-scales of X and Y are similar. However, note that we have determined the ratio $\frac{k_1}{k_2}$ earlier so the choice of k_1 and k_2 need to satisfy this ratio. Finally, for the other reaction rate constants, we make an arbitrary choice of $d_1 = k_1$ and $d_2 = k_2$, then a_1 and a_2 are computed from the definitions of H_{M1} and H_{M2} .

APPENDIX G

RHS OF (10) IS PROPORTIONAL TO THE NUMBER X_*-Y_* MOLECULES

The aim of this appendix is to show that, at steady state, the RHS of (10) is proportional to the number X_*-Y_* molecules. An assumption that we need in our proof is that the activations of X and Y by K are independent, i.e., we have:

$$\begin{aligned} & P[X-Y \text{ in state } X_*-Y_*] \\ &= P[X \text{ site in } X-Y \text{ is in } X_* \text{ state}] \times \\ & P[Y \text{ site in } X-Y \text{ is in } Y_* \text{ state}] \end{aligned} \quad (57)$$

Let $\{X - Y\}_T$ be the total number of X-Y molecules in its various states. Also, let $\{X_* - Y_*\}^{ss}$ be the steady state number of molecules in the X_*-Y_* state, X_*^{ss} (resp. Y_*^{ss}) is steady state number of molecules where the X (Y) site in the X_* (Y_*) state. We can rewrite (57) as:

$$\frac{\{X_* - Y_*\}^{ss}}{\{X - Y\}_T} = \frac{X_*^{ss}}{\{X - Y\}_T} \times \frac{Y_*^{ss}}{\{X - Y\}_T} \quad (58)$$

We now start with the RHS of (10) at steady state, which is proportional to the product of X_*^{ss} and that of the TH-function. Since we show in Appendix E that the TH-function is proportional to Y_*^{ss} , therefore, the RHS of (10) is proportional to the product $X_*^{ss}Y_*^{ss}$. By (58), we can therefore conclude that the RHS of (10) at steady state is proportional to the number of molecules in the X_*-Y_* state.

APPENDIX H

PARAMETERS OF THE TRANSMITTER AND ENZYMATIC CYCLES

For the transmitter, $r_{TX} = 3.38 \text{ s}^{-1}$ in Reaction (1). For *TX-setting-1*, Symbols 0 and 1 are generated by using, respectively, 96 and 320 mRNA molecules. For *TX-setting-2*, these numbers are changed to 32 and 96 mRNA molecules.

The parameters of the cycle (11) are: $a_1 = 0.0463$; $d_1 = 250$; $k_1 = 250$; $a_2 = 24.24$; $d_2 = 39.24$; $k_2 = 39.24$; and, $P_T = 10$.

The parameters of the cycle (13) are: $a_3 = 2 \times 10^{-4}$; $d_3 = 100$; $k_3 = 100$; $a_4 = 2 \times 10^{-6}$; $d_4 = 1$; $k_4 = 1$; $J_T = 185$; and, $\tilde{P}_T = 30$.